EUROPEAN ORGANIZATION FOR NUCLEAR RESEARCH

Physics Preliminary Summary:
First measurement of the Λ–Ξ interaction in proton–proton collisions at the LHC

ALICE Collaboration

Abstract

The first experimental information on the strong interaction between Λ and Ξ^- strange baryons is presented in this Note. The correlation function of Λ–Ξ^- and $\overline{\Lambda}$–$\overline{\Xi}^+$ pairs produced in high-multiplicity proton–proton (pp) collisions at $\sqrt{s} = 13$ TeV at the LHC is measured as a function of the relative momentum of the pair. The femtoscopy method is used to calculate the correlation function, which is then compared with theoretical expectations obtained using a meson exchange model, chiral effective field theory, and Lattice QCD calculations close to the physical point. Data support predictions of small scattering parameters while discarding versions with large ones, thus suggesting a weak Λ–Ξ^- interaction. The limited statistical significance of the data does not yet allow one to constrain the effects of coupled channels like Σ–Ξ and N–Ω.

1 Introduction

Understanding the strong interaction among hadrons with strange quarks is one of the main challenges faced by nuclear physics at low energies. Recent theoretical developments, in parallel with the improvement of computing facilities, enabled Lattice QCD calculations close to the physical point for systems rich in strangeness [1–4]. In contrast to other approaches describing hadron–hadron interactions, such first principles calculations become more stable the higher the (quark) masses involved, and they are expected to deliver reliable results for the interaction of hadrons involving several strange quarks. On the experimental side, data are scarce for hadron–hadron interactions in the strangeness $|S| > 1$ sector due to the difficulties of producing hyperons in large amounts and the fact that those are unstable particles. Hence, the interest in this sector resides in delivering precise data in order to test the ab-initio calculations.

The study of baryon–baryon interactions with strangeness is also crucial for the search of possible di-baryon states beyond the deuteron. One debated case is the NΩ state predicted by Lattice QCD calculations [3] and meson exchange models [5]. It would be held together by an attractive strong interaction at all distances favored by the absence of Pauli blocking in this system. Two-particle correlation studies of p–Ω⁻ [6, 7] show that drawing a firm conclusion on its existence is a difficult task due to the complexity of this system that arises from the coupling to several other channels. It has been demonstrated in Ref. [8] that the presence of coupled channels modifies the correlation function, in particular in the case of systems size of the order of 1 fm, such as those produced in ppcollisions. The thresholds of the Λ–Ξ and the Σ–Ξ channels lie around 180 and 90 MeV/c^2 below the N–Ω threshold, respectively; the influence of those channels could severely modify the p–Ω⁻ correlation function [9, 10] depending on the coupling strength and the characteristics of the Λ–Ξ and the Σ–Ξ interactions themselves. The investigation of those channels is thus mandatory in order to clarify the existence of the NΩ bound state.

Besides the first principles calculations, in the sector of nucleon–hyperon (N–Y) and hyperon–hyperon (Y–Y) interactions with strangeness content $|S| \leq 3$, several predictions from different theoretical approaches are waiting for validation since over a decade. Leading order (LO) chiral Effective Field Theory (χEFT) [11], meson exchange models [12], and quark constituent models [13] produced predictions for the $|S| \leq 2$ sectors relying on SU(3) symmetry considerations. Those approaches were anchored to the vast database available in the N–N sector, which includes precise determination of scattering cross sections that enable differential studies and partial wave analyses, to measurements of Λ–N cross sections and, to a lesser extent, to Σ–N cross sections. Very recently, the extension of NLO χEFT potentials from $S = -2$ [14, 15] to $S = -3$ and $S = -4$ systems has been explored [16]. These potentials are in accordance with the few experimental constraints on the Λ–Λ and Ξ–N interactions and account for effects from SU(3) symmetry breaking in the extension.

At the time when most of those potentials were constructed there was little hope for precise data on the interaction between baryon pairs with more than two strange quarks, and the experimental information was limited to the scarce data derived from the detection of hypernuclei, such as binding energies for double-Λ hypernuclei [17–20] and Ξ hypernuclei [21, 22]. However, binding energies alone do not allow unambiguous conclusions on the underlying baryon–baryon interactions, and so the available theoretical predictions were awaiting more demanding tests.

Only recently, the femtoscopy technique has delivered precise data with valuable information for the description of the strong interaction among hadrons via the study of two-particle correlations as a function of the relative momentum using collider experiments [23]. Measurements of multi-strange systems Λ–Λ [24–26], p–Ξ⁻ [27], and p–Ω⁻ [6, 7] have been made available from Au–Au collisions at RHIC by STAR and from pp collisions at the LHC by ALICE.

A pioneering study with the first experimental information of the Λ–Ξ⁻ interaction is presented in this Note. This measurement constitutes the first benchmark for models and theoretical approaches delivering

predictions for this system.

2 Data analysis

The analysis of the correlation function of Λ–Ξ$^-$ and $\overline{\Lambda}$–$\overline{\Xi}^+$ pairs is performed in the sample of high-multiplicity pp collisions at $\sqrt{s}$ = 13 TeV collected by ALICE [28, 29] at the LHC during the Run 2 period. The V0 detector of the ALICE apparatus is used for event selection and triggering. The V0 detector consists of two plastic scintillator arrays located on both sides of the collision vertex at pseudorapidities $2.8 < \eta < 5.1$ and $-3.7 < \eta < -1.7$ [30]. In order to guarantee an uniform acceptance at midrapidity, events are accepted for analysis if the reconstructed primary interaction vertex position along the beam axis (V_z) is located no more than 10 cm away from the nominal interaction point. In addition, a V0-based high-multiplicity trigger is used for selecting events in which the detected signal amplitude exceeds a defined threshold corresponding to the 0.17% highest-multiplicity events out of all inelastic collisions with at least one measured charged particle within $|\eta| < 1$ (INEL> 0). The resulting average charged-particle multiplicity density at midrapidity ($|\eta| < 0.5$) is about $\langle dN_{ch}/d\eta \rangle = 30$. An enhanced production of hyperons was reported for such high-multiplicity events [31], which provides an abundant sample of hyperons for this analysis.

Strange baryon reconstruction is performed using topological properties of their weak decays, which in turn employs the tracking and particle identification capabilities of the ALICE detector. The Inner Tracking System (ITS) and the Time-Projection Chamber (TPC) are used for charged-particle tracking and momentum reconstruction, the TPC is used as well for particle identification (PID), and the Time-of-Flight detector (TOF) is used for timing information. The ITS, TPC, and TOF are immersed in a uniform magnetic field along the beam direction with a strength of 0.5 T. The ITS [32] is made up of six layers of high position-resolution silicon detectors placed at a radial distance between 3.9 and 43 cm around the beam pipe. The TPC [33] is a 5 m long gaseous cylindrical detector covering the whole azimuth within the pseudorapidity range $|\eta| < 0.9$. It performs PID by measuring the specific energy loss (dE/dx). The TOF [34] consists of Multigap Resistive Plate Chambers which cover the full azimuth range at $|\eta| < 0.9$. Combinatorial background from out-of-bunch collision pile-up in the TPC is suppressed by rejecting charged tracks unless a matched hit in the ITS, which does not have out-of-bunch pile-up, or in the TOF, with timing information, is present.

The Λ ($\overline{\Lambda}$) are identified exploiting their characteristic V-shaped weak decay $\Lambda \rightarrow p + \pi^-$ and $\overline{\Lambda} \rightarrow \overline{p} + \pi^+$, henceforth denoted "V^0" decays, and selected within an invariant mass window of 4 MeV/c^2 around the Λ nominal mass. Proton and pion tracks are reconstructed using the TPC, and they are identified through the TPC dE/dx measurement. They are further combined into V^0 candidates if a certain pair of proton and pion tracks passes a set of geometrical criteria that ensures their consistency with the desired decay topology. These include a selection on the distance of closest approach (DCA) of the two tracks, the cosine of the pointing angle (CPA) between the line connecting the primary vertex with the candidate's decay vertex and its momentum, and the decay radius. Furthermore, a minimal transverse momentum of $p_T \geq 0.3$ MeV/c is required for the Λ ($\overline{\Lambda}$) candidates.

The Ξ$^-$ ($\overline{\Xi}^+$) candidates are identified via the weak decay channel $\Xi^- \rightarrow \Lambda + \pi^-$ and $\overline{\Xi}^+ \rightarrow \overline{\Lambda} + \pi^+$ by combining V^0 candidates with a third track with a TPC energy loss signature that is consistent with the pion mass hypothesis. They are selected within an invariant mass window of 5 MeV/c^2 around the nominal Ξ$^-$ mass. Also in this case, geometric selections serve to identify the expected trajectory arrangement and include standard Λ and $\overline{\Lambda}$ selections as well as a DCA between the V^0 and the third track and a CPA of the Ξ candidate momentum with respect to the estimated decay position. Also the Ξ$^-$ ($\overline{\Xi}^+$) candidates are required to have a minimal transverse momentum of $p_T \geq 0.3$ MeV/c. Candidates are rejected if they are compatible within 5 MeV/c^2 with the Ω$^-$ ($\overline{\Omega}^+$) baryon invariant mass through the weak decay $\Omega^- \rightarrow \Lambda + K^-$ ($\overline{\Omega}^+ \rightarrow \overline{\Lambda} + K^+$) by assuming the kaon mass hypothesis for the third track.

The numerical values of the geometrical variables used to select $\Lambda\,(\overline{\Lambda})$ and $\Xi^-\,(\overline{\Xi}^+)$, as well as the variations of such values used to estimate the systematic uncertainties of the data, are based on previous analyses; see Ref. [25] and Ref. [35] for $\Lambda\,(\overline{\Lambda})$ and $\Xi^-\,(\overline{\Xi}^+)$, respectively. A fit to the invariant mass spectrum of $\Lambda\,(\overline{\Lambda})$ and $\Xi^-\,(\overline{\Xi}^+)$ candidates is performed using a double Gaussian to describe the signal and a first-order polynomial for the combinatorial background. For the calculation of the invariant mass of $\Lambda\,(\overline{\Lambda})$ the pion and proton hypothesis are used for the daughter tracks; in the case of $\Xi^-\,(\overline{\Xi}^+)$ the $\Lambda\,(\overline{\Lambda})$ mass is used for the V^0 and the pion mass for the charged track. The results of the fit deliver average mass resolutions of around 1.5 and 2 MeV/c^2 and purities of 95% and 92% for $\Lambda\,(\overline{\Lambda})$ and $\Xi^-\,(\overline{\Xi}^+)$, respectively.

Events are kept for further analysis if at least one $\Lambda\,(\overline{\Lambda})$ and one $\Xi^-\,(\overline{\Xi}^+)$ candidate are reconstructed, which results in a total number of 8.57×10^6 events and 5.08×10^6 (4.75×10^6) Λ–Ξ^- $(\overline{\Lambda}$–$\overline{\Xi}^+)$ pairs.

During the reconstruction, a charged track can be assigned as a decay product of multiple V^0 candidates. For such cases, an additional selection procedure is implemented to reduce the combinatorial background and choose the best candidate in an unbiased way. The V^0 candidates that share a charged track are discriminated by using several kinematic variables simultaneously, namely the invariant mass, the DCA, and the CPA. They are compared to template distributions from Monte Carlo (MC) simulations and normalized by their expected resolution such that they have the same incidence in the comparison. For the MC templates, pp events are generated using PYTHIA 8.2 [36] and the resulting particles are propagated through the simulation of the ALICE detector using GEANT3 [37]. An analogous track cleaning procedure is used as well for the Ξ candidates that share charged tracks. The track cleaning procedure reduces the sample of Ξ^- and $\overline{\Xi}^+$ candidates by 0.6% and the sample of Λ and $\overline{\Lambda}$ candidates by 1.9%.

In order to avoid autocorrelations generated by the pairing of $\Lambda\,(\overline{\Lambda})$ candidates with their mother particles, pairs of Λ–Ξ^- $(\overline{\Lambda}$–$\overline{\Xi}^+)$ are not considered if the $\Lambda\,(\overline{\Lambda})$ candidate shares any charged track with the $\Xi^-\,(\overline{\Xi}^+)$ candidate.

3 Correlation function

Experimentally, the two-particle correlation function is defined as [38]

$$C(k^*) = \mathcal{N} \times \frac{N_{\text{same}}(k^*)}{N_{\text{mixed}}(k^*)}\,, \tag{1}$$

where k^* is the relative momentum in the pair rest frame, defined as $k^* = \frac{1}{2} \times |\mathbf{p}_1^* - \mathbf{p}_2^*|$ with $\mathbf{p}_i$ being the three-momenta of the involved particle candidates. The N_{same} is the k^* distribution of particle pairs produced in the same collision, whereas N_{mixed} is the k^* distribution obtained by pairing particles produced in different collisions with similar V_z and multiplicity. Due to the event mixing procedure, the number of pairs in N_{mixed} is higher than in N_{same}, hence the correlation function has to be normalized at large k^*, where the effects of the final state interactions are absent. This is denoted by the factor $\mathcal{N}$; the normalization is performed in the region $k^* \in [450, 650]$ MeV/c. In the following, Λ–Ξ^- is used to refer to the sum of Λ–Ξ^- and $\overline{\Lambda}$–$\overline{\Xi}^+$ pairs, since both experience the same interaction and correlation and no significant differences are observed between both pairs during the analysis. A total of 6142 Λ–Ξ^- pairs are found with k^* below 200 MeV/c.

On the theoretical side, the correlation function can be expressed as a function of the particle emitting source $S(r^*)$ and the two-particle pair wave function $|\Psi(r^*, k^*)|$ which contains the interaction component [38]

$$C(k^*) = \int \mathrm{d}^3 r^* S(r^*) |\Psi(r^*, k^*)|^2\,, \tag{2}$$

where r^* refers to the relative distance between the two particles. The source function is assumed to have

a Gaussian shape. Its size is obtained from the universal baryon–baryon transverse mass (m_T) scaling observed in pp collisions [39], and considering its enlargement due to shortly lived resonances [39]. The average transverse mass of Λ–Ξ$^-$ pairs with $k^* < 200$ MeV/c is $\langle m_T \rangle = 2.01$ GeV/c^2, which leads to an effective source radius of $r_{\text{eff}} = 1.032^{+0.055}_{-0.056}$ fm. The quoted uncertainties take into account the statistical and systematic uncertainties of the parametrization of the m_T dependence [39].

Given the source size, the theoretical correlation function is computed using two different methods. The Lednický–Lyuboshits (LL) approach [40, 41] allows one to calculate the theoretical correlation function when the effective range parameters are known: scattering length f_0^s and effective range d_0^s, with s denoting the spin state of the pair. Note that in this Note the standard notation and sign convention in femtoscopy is used, where a positive f_0 corresponds to an attractive interaction, while a negative scattering length corresponds either to a repulsive potential or a bound state. For Λ–Ξ$^-$ pairs, there are two spin configurations, namely a singlet with $s = 0$ and a triplet with $s = 1$. They contribute with a weight of 1/4 and 3/4 to the total theoretical correlation function, respectively. The LL model is used to evaluate the predictions from the Nijmegen meson exchange model [12] and the interactions from χEFT [11, 16]. The second method uses the CATS framework [42], a Schrödinger equation solver, to evaluate the wave functions for the potentials extracted from Lattice QCD calculations performed by the HAL QCD Collaboration [2].

The Λ–Ξ$^-$ correlation functions evaluated for the central value of the radius r_{eff} for each considered theoretical prediction are shown in Fig.1. Since the Coulomb interaction is absent, the deviations from unity at small relative momentum are exclusively due to the strong interaction. Details on the characteristics of each interaction are discussed in Section 4.
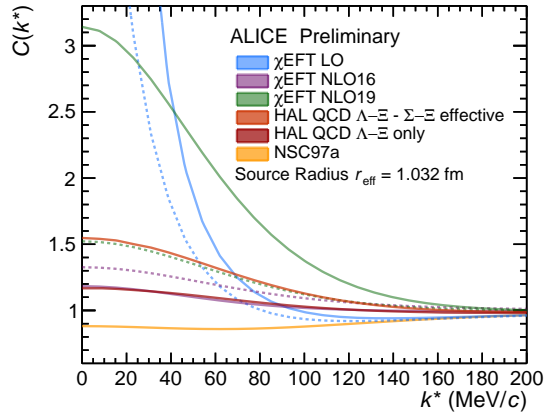

Fig. 1: Theoretical Λ–Ξ$^-$ correlation functions from predictions ([2, 11, 12, 16]) evaluated for the experimental source radius. See text for details. In the case of the LO and NLO χEFT potentials the solid (dotted) lines correspond to the lowest (highest) cutoff [11, 16].

The experimental correlation function contains additional contributions to the genuine Λ–Ξ$^-$ strong interaction as it is defined in Eq. 2. In order to compare the theoretical expectations with the experimental data, a model is built for each theoretical prediction containing all contributions to the experimental correlation function as detected by ALICE

$$C_{\text{model}}(k^*) = C_{\text{non-femto}}(k^*) \times \left[\sum_i \lambda_i \times C_i(k^*) \right], \tag{3}$$

where the sum contains all femtoscopic contributions $C_i(k^*)$ namely the genuine as well as contamination induced by the misidentification background and feed-down. Each of them is multiplied with its relative

contribution λ_i. The $C_{\text{non-femto}}(k^*)$ describes non-femtoscopic effects such as energy conservation which are dominant for large k^*. It is modelled phenomenologically by a polynomial with a constant and a third degree term $C_{\text{non-femto}}(k^*) = a \times (1 - b \times k^{*3})$, which ensures a flat behaviour at $k^* \to 0$, and is fitted to the measured correlation function.

In the feed-down contributions, at least one particle of the pair originates from a decay and appears on timescales larger than the strong interaction which is measured here. They carry the residual correlation from their mother particle which is washed out because of the decay. The main feed-down to the Λ ($\overline{\Lambda}$) candidates comes from the Ξ^- ($\overline{\Xi}^+$), Ξ^0 ($\overline{\Xi}^0$), and Σ^0 ($\overline{\Sigma}^0$) decays. The combined relative contribution is obtained by fitting the CPA distribution to MC templates. Then, the λ parameter for each contribution is determined via isospin considerations. The feed-down to the Ξ^- ($\overline{\Xi}^+$) candidates comes from the decays of the resonances $\Xi^-(1530)$ and $\Xi^0(1530)$ as well as the Ω^- ($\overline{\Omega}^+$) hyperons. Their λ parameters are extracted from the production rates reported in Refs. [31, 43] and their branching ratios [44]. All feed-down contributions to the correlation function are assumed to be constant in k^* with a value equal to unity, except for the case of the $\Xi^- - \Xi^-$ feed-down, with the identified Λ coming from the decay of an unidentified Ξ^-. The latter contributes with $\lambda_{\Xi^- - \Xi^-} = 8\%$; it is modelled assuming a pure Coulomb $\Xi^- - \Xi^-$ interaction and it is propagated to $C_{\text{model}}(k^*)$ via a momentum transformation from the $\Xi^- - \Xi^-$ to the Λ–Ξ^- pair rest frame. The relative contribution of all the other feed-down contributions is of $\lambda_{\text{flat}} = 48\%$.

The relative contribution from misidentification is of $\lambda_{\text{mis.}} = 12\%$ and is calculated from the purities in the selection of the Λ and Ξ^-. This contribution is modelled by a second order polynomial $C_{\text{mis.}}(k^*) = p_0 + p_1 k^* + p_2 k^{*2}$ with parameters obtained via a fit to the correlation function constructed using Λ–Ξ^- pairs from an invariant mass sideband analysis [45]. The values of the parameters are $p_0 = 1.22$, $p_1 = -8.94 \times 10^{-4}$ $(\text{MeV}/c)^{-1}$, and $p_2 = 8.90 \times 10^{-7}$ $(\text{MeV}/c)^{-2}$.

The relative contribution from the genuine Λ–Ξ^- interaction is $\lambda_{\text{genuine}} = 32\%$. In order to consider the finite momentum resolution, evaluated via full simulations of the ALICE apparatus and its response, $C_{\text{model}}(k^*)$ has to be transformed into the basis of the reconstructed momenta as it was done in previous analysis [25].

4   Results

The experimental Λ–Ξ^- correlation function is shown in Fig. 2 in two different k^* and $C(k^*)$ ranges. The systematic uncertainties of the data displayed in Fig. 2 are associated with variations on the selection criteria of Λ ($\overline{\Lambda}$) and Ξ^- ($\overline{\Xi}^+$) as explained in Section 2. The analysis is repeated with 39 random combinations of such variations. For each k^* point, the final systematic uncertainty is given by the width of a Gaussian fit including all 39 measurements of the correlation function.

The data are compared in Fig. 2 with predictions of the correlation function, according to Eq. 3, from several theoretical descriptions of the Λ–Ξ^- strong interaction and from the assumption of no interaction. The parameter of the non-femtoscopic baseline is fitted to the data for each case in the range $k^* \in [0, 800]$ MeV/c. The width of the theoretical bands reflect the uncertainties in the evaluation of the correlation function, namely: i) variations of the radius of the source function according to the experimental determination $r_{\text{eff}} = 1.032^{+0.055}_{-0.056}$ fm; ii) variation of the normalization range by ± 50 MeV/c; iii) variation of the range of the fit to the non-femtoscopic baseline by ± 50 MeV/c; iv) variation in the parametrization of the baseline using a second order polynomial (i.e. the non-femto contribution becomes $C_{\text{non-femto}}(k^*) = a' \times (1 - b' \times k^{*2})$); and v) variation of the functional form describing the sidebands correlation function to $p_0 + \exp(p_1 + p_2 k^*)$. The evaluation of the theoretical correlation function and the fit of the baseline parameters were performed with all possible combinations of such variations. The width of the theoretical band for each model is given in each k^* point by the root mean squared of all fit results.

The dotted black line in Fig. 2 represents the result of the baseline fit assuming no Λ–Ξ$^-$ strong interaction, for which $a = 0.95$ and $b = 2.4 \times 10^{-10}$ (MeV/c)$^{-3}$ are obtained. The compatibility with the data is evaluated in terms of the number of standard deviations n_σ, which were obtained from the p-value computed in the range $k^* < 200$ MeV/c. The uncertainties of the data were considered by adding the statistical and systematic uncertainties in quadrature. The result for the "no strong interaction" assumption is $n_\sigma = 0.78$ showing that in the low relative momentum region, where femtoscopic effects are expected, data do not deviate significantly from the baseline.
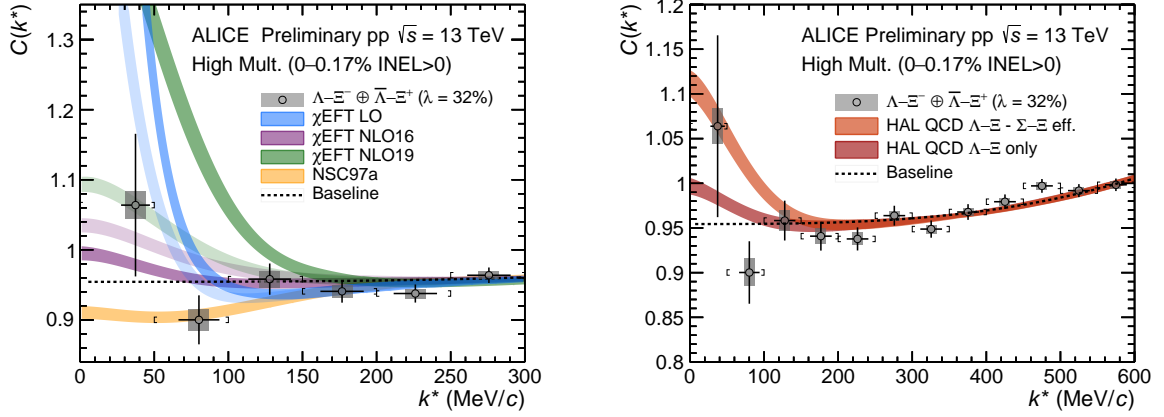

Fig. 2: Experimental Λ–Ξ$^-$ correlation function with statistical (vertical black lines) and systematic (gray boxes) uncertainties. The square brackets show the bin width of the measurement and the horizontal black lines represent the statistical uncertainty in the determination of the mean k^* for each bin. Left panel: Comparison to LO [11] and NLO [16] χEFT and NSC97a [12] potentials evaluated with the Lednický–Lyuboshits model [40, 41]. In the χEFT models the darker and light version corresponds to the version with the lower and higher cut-off value, respectively. Right panel: Comparison with Lattice QCD calculations by the HAL QCD Collaboration [2] using an effective potential including the coupling to Σ–Ξ (orange) and the Λ–Ξ$^-$ elastic potential alone (red). The width of the bands in both panels correspond to the systematic uncertainties of the fit as described in the text. The baseline is the average baseline of all fit variations and models.

The dark blue and light blue bands in the left panel of Fig. 2 represent the correlation function evaluated from LO χEFT [11] for a regulator function cut-off of 550 and 700 MeV, respectively. The genuine Λ–Ξ$^-$ correlation function is evaluated by using the LL model with the scattering parameters for ΛΞ provided in Ref. [11]. The scattering length in this case indicates a rather strong attraction in the singlet channel and a mild repulsion in the triplet channel. The predicted values depend strongly on the cut-off choice, which is reflected in the correlation function. The curve corresponding to the LO χEFT potential with 550 MeV cut-off, with rather large scattering length, is not compatible with the experimental correlation function. On the other hand, the result for the potential with cut-off 700 MeV is close to the data. However, this interaction implies the presence of a shallow ΛΞ bound state with a binding energy of just 0.43 MeV. Such bound states are not seen anymore in the extrapolation of the NLO interactions from $S = -2$ [14, 15] to $S = -3$ [16], where effects from SU(3) symmetry breaking have been properly accounted for, in line with the power counting. They are also not supported by the available lattice QCD simulations close to the physical point [2]. The correlation functions expected from the NLO calculations, based on NLO16 [14] and NLO19 [15], are represented by the magenta and green bands in the left panel of Fig. 2, respectively. The dark and light bands represent the interactions with regulator function cut-offs of 500 and 650 MeV, respectively, for both potentials. The correlation function was evaluated by using the LL model with the scattering lengths[1] provided in Ref. [16]. The NLO19 potential

---

[1]For the triplet state in NLO16 the effective range is set to $d_0 = 0$ fm. This is necessary since the LL does not provide stable results for the large effective ranges predicted by the theory (see Table 1) in combination with the small source radius.

is more attractive than the NLO16 in the triplet channel, and there is also a sizable cut-off dependence. This is reflected in a larger correlation function, in particular for the 500 MeV cut-off (dark green band), that clearly exceeds the data. This demonstrates that the ALICE data delivers important constraints in the $S = -3$ sector needed to fix the free parameters in the χEFT NLO calculations [16].

The Nijmegen meson exchange model [12] predicts the existence of a Σ–Ξ bound state, though in the case of the Λ–Ξ^- channel, for 5 of the 6 different versions of the model, a mild attraction and a mild repulsion in the singlet and triplet configurations, respectively, are predicted. The light orange band in Fig. 2 shows the expectation from the version NSC97a. The substantially smaller scattering lengths in the singlet state compared to the χEFT potentials are reflected in a suppressed correlation function that agrees with the data.

It is worth mentioning that the scattering parameters from the quark constituent model *fss2* [13] coincide qualitatively with the Nijmegen potential, although that model does not predict any Σ–Ξ or Λ–Ξ^- bound states.

The right panel of Fig. 2 shows the comparison with the results for the HAL QCD Λ–Ξ^- potential [2]. The width of the HAL QCD curves include statistical and systematic variations of the lattice calculations following the recipe in Ref. [7]. The HAL QCD potential is a $\Lambda\Xi$–$\Sigma\Xi$ coupled-channel potential. It presents attraction in both the singlet and the triplet configurations but does not predict the formation of any bound state. The orange curve shows the results from an effective Λ–Ξ^- potential, where the coupling to Σ–Ξ from the lattice simulations is incorporated effectively into the strength of the Λ–Ξ^- interaction. For reference, the red curve shows the correlation function from the $\Lambda\Xi$–$\Lambda\Xi$ elastic potential alone, free of effects from the coupling. The difference between the orange and red curves in Figs. 2 and 1 demonstrates a rather strong coupling. This is particularly noticeable if the results are compared to the HAL QCD pΞ–$\Lambda\Lambda$ potential in the $|S| = 2$ sector [1], in which case the coupling between channels is small and has negligible effects in the correlation function [46]. While the ALICE data shows better compatibility with the single channel $\Lambda\Xi$–$\Lambda\Xi$ elastic potential, it is not sensitive to the effects of the coupling as shown by Lattice QCD.

Threshold cusp-like structures at the channel opening created by the inelastic channels could be formed [47] with an amplitude depending on the properties of the interaction, the strength of the coupling between channels, and the amount of initial state pairs in the inelastic channels. The ALICE data do not present significant structures at the kinematic opening of the Σ^-–Ξ^0, Σ^0–Ξ^- and n–Ω^- channels, at k^* values of 303, 308 and 468 MeV/c respectively.

The scattering parameters of all considered interactions are summarized in Table 1, together with the compatibility of each of them with the Λ–Ξ^- correlation function in terms of n_σ computed in the range $k^* < 200$ MeV/c, considering the statistical and systematic uncertainties of the data. The scattering parameters of the HAL QCD calculations were extracted using CATS by fitting the phase shifts δ_0 with the effective range approximation [48, 49].

Summary

This Note presents the first measurement of the Λ–Ξ^- interaction, quantified via the correlation function $C(k^*)$ in high-multiplicity pp collisions at $\sqrt{s} = 13$ TeV. The measured $C(k^*)$ were compared with different descriptions of the Λ–Ξ^- interaction, including leading-order and next-to-leading-order chiral Effective Field Theory calculations, a meson exchange model, and recent Lattice QCD calculations. Despite the limited statistical significance and the contamination from feed-down contributions, the data provide the first constraint for theoretical investigations and are seen to be more compatible with predictions of small scattering parameters and hence a weak Λ–Ξ^- interaction. The limitations of the data sample prevent from drawing further conclusions on the influence of coupled channels in the correlation

Table 1: Summary of scattering parameters and agreement with the data in terms of n_σ of the considered interactions. The effective range parameters for the Lattice QCD results are obtained from the low-energy phase shifts which are extracted with CATS in the evaluation of the potentials. The agreement of the baseline (no interaction assumed) is also given.

potential	cut-off (MeV) / version	singlet		triplet		n_σ
		f_0^0	d_0^0	f_0^1	d_0^1	
χEFT LO [11]	550	33.5	1.00	-0.33	-0.36	$3.06 - 5.12$
	700	-9.07	0.87	-0.31	-0.27	$0.78 - 1.60$
χEFT NLO16 [14]	500	0.99	5.77	-0.026	142.9	$0.56 - 0.93$
	650	0.91	4.63	0.12	32.02	$0.91 - 1.61$
χEFT NLO19 [15]	500	0.99	5.77	1.66	1.49	$5.47 - 7.26$
	650	0.91	4.63	0.42	6.33	$1.30 - 2.10$
NSC97a [12]		0.80	4.71	-0.54	-0.47	$0.68 - 1.04$
HAL QCD [2]	ΛΞ–ΣΞ eff.	0.60	6.01	0.50	5.36	$1.43 - 2.34$
	ΛΞ–ΛΞ only	–	–	–	–	$0.64 - 1.04$
Baseline		–	–	–	–	0.78

function, and no significant cusp-like structures are observed at the opening of the $\Sigma^--\Xi^0$, $\Sigma^0-\Xi^-$ or n–Ω^- channels. The presented data demonstrate that the characteristics of the strong interaction in the $|S| = 3$ sector can be investigated with the femtoscopy technique. New measurements with the upgraded ALICE apparatus [50] will exploit the data collected during upcoming LHC Run 3 and Run 4 [51, 52] and should deliver a precise insight into the Λ–Ξ^- interaction, providing valuable information for the search of di-baryon states with strangeness content.

References

[1] K. Sasaki *et al.*, "ΛΛ and NΞ interactions from Lattice QCD near the physical point", *Nucl. Phys. A* **998** (2020) 121737.

[2] N. Ishii *et al.*, "Baryon interactions from lattice QCD with physical masses —S = −3 sector: ΞΣ and ΞΣ-ΛΣ—", *EPJ Web Conf.* **175** (2018) 05013.

[3] **HAL QCD** Collaboration, T. Iritani *et al.*, "NΩ dibaryon from lattice QCD near the physical point", *Phys. Lett. B* **792** (2019) 284–289, arXiv:1810.03416 [hep-lat].

[4] S. Gongyo *et al.*, "Most Strange Dibaryon from Lattice QCD", *Phys. Rev. Lett.* **120** no. 21, (2018) 212001, arXiv:1709.00654 [hep-lat].

[5] T. Sekihara, Y. Kamiya, and T. Hyodo, "NΩ interaction: meson exchanges, inelastic channels, and quasibound state", *Phys. Rev. C* **98** no. 1, (2018) 015205, arXiv:1805.04024 [hep-ph].

[6] **STAR** Collaboration, J. Adam *et al.*, "The Proton-Ω correlation function in Au + Au collisions at $\sqrt{s_{NN}} = 200$ GeV", *Phys. Lett. B* **790** (2019) 490–497, arXiv:1808.02511 [hep-ex].

[7] **ALICE** Collaboration, S. Acharya *et al.*, "Unveiling the strong interaction among hadrons at the LHC", *Nature* **588** (2020) 232–238, arXiv:2005.11495 [nucl-ex].

[8] Y. Kamiya, T. Hyodo, K. Morita, A. Ohnishi, and W. Weise, "K^-p Correlation Function from High-Energy Nuclear Collisions and Chiral SU(3) Dynamics", *Phys. Rev. Lett.* **124** no. 13, (2020) 132501, arXiv:1911.01041 [nucl-th].

[9] K. Morita, A. Ohnishi, F. Etminan, and T. Hatsuda, "Probing multistrange dibaryons with proton-omega correlations in high-energy heavy ion collisions", *Phys. Rev. C* **94** no. 3, (2016) 031901, arXiv:1605.06765 [hep-ph]. [Erratum: Phys.Rev.C 100, 069902 (2019)].

[10] K. Morita, S. Gongyo, T. Hatsuda, T. Hyodo, Y. Kamiya, and A. Ohnishi, "Probing $\Omega\Omega$ and $p\Omega$ dibaryons with femtoscopic correlations in relativistic heavy-ion collisions", *Phys. Rev. C* **101** (2020) 015201, arXiv:1908.05414 [nucl-th].

[11] J. Haidenbauer and U.-G. Meißner, "Predictions for the strangeness S = -3 and -4 baryon-baryon interactions in chiral effective field theory", *Phys. Lett. B* **684** (2010) 275–280, arXiv:0907.1395 [nucl-th].

[12] V. G. J. Stoks and T. A. Rijken, "Soft core baryon baryon potentials for the complete baryon octet", *Phys. Rev. C* **59** (1999) 3009–3020, arXiv:nucl-th/9901028.

[13] Y. Fujiwara, Y. Suzuki, and C. Nakamoto, "Baryon-baryon interactions in the SU(6) quark model and their applications to light nuclear systems", *Prog. Part. Nucl. Phys.* **58** (2007) 439–520, arXiv:nucl-th/0607013.

[14] J. Haidenbauer, U.-G. Meißner, and S. Petschauer, "Strangeness S = −2 baryon–baryon interaction at next-to-leading order in chiral effective field theory", *Nucl. Phys. A* **954** (2016) 273–293, arXiv:1511.05859 [nucl-th].

[15] J. Haidenbauer and U.-G. Meißner, "In-medium properties of a ΞN interaction derived from chiral effective field theory", *Eur. Phys. J. A* **55** no. 2, (2019) 23, arXiv:1810.04883 [nucl-th].

[16] J. Haidenbauer and U.-G. Meißner, "Strangeness $S = −3$ and $−4$ baryon-baryon interactions in chiral effective field theory", in *10th International workshop on Chiral Dynamics*. 1, 2022. arXiv:2201.08238 [nucl-th].

[17] M. Danysz *et al.*, "The identification of a double hyperfragment", *Nucl. Phys.* **49** (1963) 121–132.

[18] H. Takahashi *et al.*, "Observation of a $^{6}_{\Lambda\Lambda}$He double hypernucleus", *Phys. Rev. Lett.* **87** (2001) 212502.

[19] **KEK E176** Collaboration, S. Aoki *et al.*, "Nuclear capture at rest of Ξ^- hyperons", *Nucl. Phys. A* **828** (2009) 191–232.

[20] **E373 (KEK-PS)** Collaboration, J. K. Ahn *et al.*, "Double-Λ hypernuclei observed in a hybrid emulsion experiment", *Phys. Rev. C* **88** no. 1, (2013) 014003.

[21] K. Nakazawa *et al.*, "The first evidence of a deeply bound state of $\Xi^- - {}^{14}$N system", *PTEP* **2015** (2015) 033D02.

[22] **J-PARC E07** Collaboration, S. H. Hayakawa *et al.*, "Observation of Coulomb-Assisted Nuclear Bound State of $\Xi^- - {}^{14}N$ System", *Phys. Rev. Lett.* **126** no. 6, (2021) 062501, arXiv:2010.14317 [nucl-ex].

[23] L. Fabbietti, V. M. Sarti, and O. V. Doce, "Study of the strong interaction among hadrons with correlations at the LHC", *Ann. Rev. Nucl. Part. Sci.* **71** (2021) 377–402, arXiv:2012.09806 [nucl-ex].

[24] **STAR** Collaboration, L. Adamczyk *et al.*, "$\Lambda\Lambda$ Correlation Function in Au+Au collisions at $\sqrt{s_{\mathrm{NN}}} = 200$ GeV", *Phys. Rev. Lett.* **114** (2015) 022301, arXiv:1408.4360 [nucl-ex].

[25] **ALICE** Collaboration, S. Acharya *et al.*, "p-p, p-Λ and Λ-Λ correlations studied via femtoscopy in pp reactions at $\sqrt{s} = 7$ TeV", *Phys. Rev. C* **99** (2019) 024001, arXiv:1805.12455 [nucl-ex].

[26] **ALICE** Collaboration, S. Acharya *et al.*, "Study of the Λ–Λ interaction with femtoscopy correlations in pp and p–Pb collisions at the LHC", *Phys. Lett. B* **797** (2019) 134822, arXiv:1905.07209 [nucl-ex].

[27] **ALICE** Collaboration, S. Acharya *et al.*, "First Observation of an Attractive Interaction between a Proton and a Cascade Baryon", *Phys. Rev. Lett.* **123** (2019) 112002, arXiv:1904.12198 [nucl-ex].

[28] **ALICE** Collaboration, K. Aamodt *et al.*, "The ALICE experiment at the CERN LHC", *JINST* **3** (2008) S08002.

[29] **ALICE** Collaboration, B. Abelev *et al.*, "Performance of the ALICE Experiment at the CERN LHC", *Int. J. Mod. Phys.* **A29** (2014) 1430044.

[30] **ALICE** Collaboration, E. Abbas *et al.*, "Performance of the ALICE VZERO system", *JINST* **8** (2013) P10016, arXiv:1306.3130 [nucl-ex].

[31] **ALICE** Collaboration, J. Adam *et al.*, "Enhanced production of multi-strange hadrons in high-multiplicity proton-proton collisions", *Nature Phys.* **13** (2017) 535–539, arXiv:1606.07424 [nucl-ex].

[32] **ALICE** Collaboration, K. Aamodt *et al.*, "Alignment of the ALICE Inner Tracking System with cosmic-ray tracks", *JINST* **5** (2010) P03003, arXiv:1001.0502 [physics.ins-det].

[33] J. Alme *et al.*, "The ALICE TPC, a large 3-dimensional tracking device with fast readout for ultra-high multiplicity events", *Nucl. Instrum. Meth. A* **622** (2010) 316–367, arXiv:1001.1950 [physics.ins-det].

[34] A. Akindinov *et al.*, "Performance of the ALICE Time-Of-Flight detector at the LHC", *Eur. Phys. J. Plus* **128** (2013) 44.

[35] **ALICE** Collaboration, K. Aamodt *et al.*, "Strange particle production in proton-proton collisions at sqrt(s) = 0.9 TeV with ALICE at the LHC", *Eur. Phys. J. C* **71** (2011) 1594, arXiv:1012.3257 [hep-ex].

[36] T. Sjöstrand, S. Ask, J. R. Christiansen, R. Corke, N. Desai, P. Ilten, S. Mrenna, S. Prestel, C. O. Rasmussen, and P. Z. Skands, "An introduction to PYTHIA 8.2", *Computer Physics Communications* **191** (2015) 159–177, arXiv:1410.3012 [hep-ph].

[37] R. Brun, R. Hagelberg, M. Hansroul, and J. C. Lassalle, *Simulation program for particle physics experiments, GEANT: user guide and reference manual.* CERN, Geneva, 1978. https://cds.cern.ch/record/118715.

[38] M. A. Lisa, S. Pratt, R. Soltz, and U. Wiedemann, "Femtoscopy in relativistic heavy ion collisions: Two Decades of Progress", *Ann. Rev. Nucl. Part. Sci.* **55** (2005) 357–402, arXiv:nucl-ex/0505014 [nucl-ex].

[39] **ALICE** Collaboration, S. Acharya *et al.*, "Search for a common baryon source in high-multiplicity pp collisions at the LHC", *Phys. Lett. B* **811** (2020) 135849, arXiv:2004.08018 [nucl-ex].

[40] R. Lednicky and V. Lyuboshits, "Final State Interaction Effect on Pairing Correlations Between Particles with Small Relative Momenta", *Sov. J. Nucl. Phys.* **35** (1982) 770.

[41] A. Stavinskiy, K. Mikhailov, B. Erazmus, and R. Lednický, "Residual correlations between decay products of $\pi^0\pi^0$ and $p\Sigma^0$ systems", arXiv:0704.3290 [nucl-th].

[42] D. Mihaylov, V. Mantovani Sarti, O. Arnold, L. Fabbietti, B. Hohlweger, and A. Mathis, "A femtoscopic Correlation Analysis Tool using the Schrödinger equation (CATS)", *Eur. Phys. J. C* **78** (2018) 394, arXiv:1802.08481 [hep-ph].

[43] **ALICE** Collaboration, B. Abelev *et al.*, "Production of $\Sigma(1385)^{\pm}$ and Ξ^0 (1530) in proton–proton collisions at $\sqrt{s} = 7$ TeV", *The European Physical Journal C* **75** (2015) 1, `arXiv:1406.3206` `[nucl-th]`.

[44] **Particle Data Group** Collaboration, P. A. Zyla *et al.*, "Review of Particle Physics", *Progress of Theoretical and Experimental Physics* **2020** no. 8, (08, 2020) .

[45] **ALICE** Collaboration, S. Acharya *et al.*, "Investigation of the p–Σ^0 interaction via femtoscopy in pp collisions", *Phys. Lett. B* **805** (2020) 135419, `arXiv:1910.14407` `[nucl-ex]`.

[46] Y. Kamiya, K. Sasaki, T. Fukui, T. Hyodo, K. Morita, K. Ogata, A. Ohnishi, and T. Hatsuda, "Femtoscopic study of coupled-channel $N\Xi$ and $\Lambda\Lambda$ interactions", YITP-21-79, RIKEN-iTHEMS-Report-21, NITEP 116, `arXiv:2108.09644` `[hep-ph]`.

[47] J. Haidenbauer, "Coupled-channel effects in hadron–hadron correlation functions", *Nucl. Phys. A* **981** (2019) 1–16, `arXiv:1808.05049` `[hep-ph]`.

[48] J. J. Sakurai and J. Napolitano, *Modern Quantum Mechanics*, pp. 388–400. Cambridge University Press, 2 ed., 2017.

[49] D. Griffiths, *Introduction to Quantum Mechanics*, pp. 394–407. Pearson international edition. Pearson Prentice Hall, 2005.

[50] **ALICE** Collaboration, B. Abelev *et al.*, "Upgrade of the ALICE Experiment: Letter Of Intent", *J. Phys. G* **41** (2014) 087001.

[51] Z. Citron *et al.*, "Report from Working Group 5: Future physics opportunities for high-density QCD at the LHC with heavy-ion and proton beams", *CERN Yellow Rep. Monogr.* **7** (2019) 1159–1410.

[52] **ALICE** Collaboration, S. Acharya *et al.*, "Future high-energy pp programme with ALICE", ALICE-PUBLIC-2020-005, CERN-LHCC-2020-018. `https://cds.cern.ch/record/2724925`.